

Topological bulk currents in topological insulators

Chris N. Self^{†,1}, Alvaro Rubio-García^{†,2}, Juan Jose García-Ripoll,³ and Jiannis K. Pachos¹

¹*School of Physics and Astronomy, University of Leeds, Leeds LS2 9JT, UK*

²*Instituto de Estructura de la Materia IEM-CSIC, Calle Serrano 123, Madrid E-28006, Spain*

³*Instituto de Física Fundamental IFF-CSIC, Calle Serrano 113b, Madrid E-28006, Spain*

(Dated: December 15, 2024)

We provide evidence that, alongside symmetry protected edge states, topological phases also support bulk currents. These currents are activated by local potential gradients even if they do not cause a phase transition. To understand their origin one can view the bulk of a homogeneous topological insulator as a perfectly entangled state of pairs of edge-like currents, adding up to a zero net flow. Local potentials strain those states, progressively disentangling the hidden currents through a transfer of population. This produces a localised bulk current that is transverse to the strain. Bulk currents are topologically protected and behave like edge currents under external influence, such as temperature or local disorder. The resilience and the tuning of bulk currents with local potentials makes them an appealing medium for technological applications.

Introduction:— When a two-dimensional topological insulator is embedded in a surface with sharp boundaries, it develops gapless symmetry protected edge states [1–5]. These edge states support currents that are robust against imperfections, conduct matter without losses and follow the direction given by a topological invariant, the Chern number. In contrast, the bulk of the material remains a gapped insulator. Topologically insulating materials have been identified experimentally [6–8] and are in fact predicted to be theoretically abundant [9–11]. An exhaustive review of inorganic crystals suggests that 12% of all recorded materials are topological insulators [9]. This abundance and the resilience of edge states make topological insulators attractive for technological applications: from frictionless, directed transport of currents, to transistors, amplifiers and detectors [12–16].

In this work we challenge the dualistic vision of edge vs. bulk states, studying how two-dimensional topological insulators behave under local and global potentials, $V(\mathbf{r})$. First, we find that the current along the edges is proportional to the potential at the boundary of the material. A uniform chemical potential $V(\mathbf{r}) = -\mu$ acting on a material with Chern number ν , produces a current

$$I_{\text{edge}} = \frac{\nu}{2\pi} \mu, \quad (1)$$

along the physical edge of the system. This current is robust against temperatures and local disorder. Most surprisingly, we find that a spatially varying potential *induces currents in the bulk of the material* without closing the gap or causing a phase transition. More precisely, any small potential gradient $\nabla V(\mathbf{r})$ induces perpendicular bulk currents

$$I_{\text{bulk}} = \frac{\nu}{2\pi} a_0 |\nabla V(\mathbf{r})|, \quad (2)$$

proportional to the Chern number ν and the lattice constant a_0 . These *bulk currents* share the topological protection of edge currents, but their strength, direction and geometry are tuneable with the potential $V(\mathbf{r})$, unconstrained by the shape of the sample.

While there is evidence of bulk currents in Dirac materials [17], our study provides the first definitive explanation that holds in a lattice. The topological bulk insulator is a many-body state of hidden entangled “edge states” that bind together, producing a zero net current. A local potential gradient strains and progressively disentangles these states, which appear as localised currents in the bulk, perpendicular to the straining gradient. In the limit of extreme potentials or when the material is cut, the edge states unbind and become free currents flowing along the sample boundary. We provide two compelling pieces of evidences for this vision: a study of 1D topological Su-Schrieffer-Heeger (SSH) model [18] under local potentials and a connection to the theory of topological insulators based on tensor-network states [19].

Edge currents in topological insulators:— We model edge physics with an isolated, one-dimensional, fermionic Hamiltonian $H = \nu \int_{-\infty}^{\infty} dp \varepsilon(p) a_p^\dagger a_p$. The annihilation and creation operators for momentum p , a_p^\dagger and a_p , obey a linear dispersion relation, $\varepsilon(p) = p$, that extends to infinity. In equilibrium at temperature T , the occupation of the edge states depends on momentum and chemical potential μ as $n(p) = (e^{(\varepsilon(p)-\mu)/T} + 1)^{-1}$. Holes in the negative energy modes are quasiparticles with positive energy and momentum, which we write as $b_p^\dagger = a_{-p}$. In units of e^2/\hbar , the net particle current is

$$I_{\text{edge}} = \frac{\nu}{2\pi} \int_0^\infty d\varepsilon [n(\varepsilon - \mu) - n(\varepsilon + \mu)]. \quad (3)$$

This integral results in Eq. (1), a current proportional to ν and μ , independent of the temperature T .

For a more realistic discussion of edge states, we turn to the Haldane model [20] for fermions $\{c_i, c_i^\dagger\}$ tunnelling

[†] CNS and AR-G contributed equally to this work.

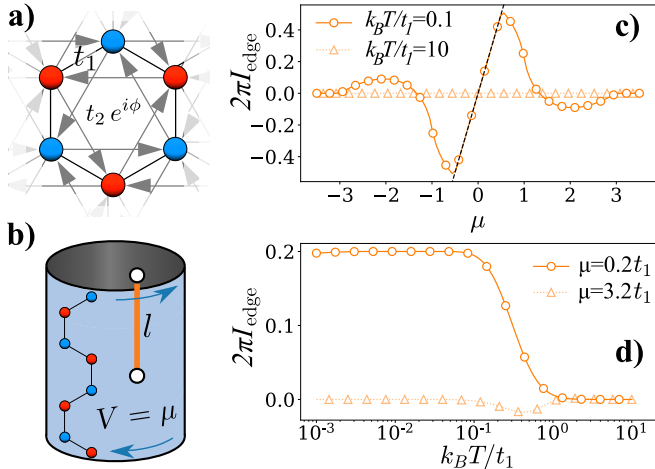


FIG. 1. Edge currents of the Haldane model as a function of temperature, T , and chemical potential, μ . (a) Hexagonal plaquette of the Haldane lattice model. Arrows denote hopping directions for which $\nu_{ij} = +1$ in Eq. (4). (b) The Haldane model on a cylinder showing the direction of the edge currents and the line l used to define I_{edge} . (c) Edge currents vs. chemical potential for $k_B T = 0.1t_1$ and $10t_1$. At low temperatures the current is independent of temperature and follows Eq. (1); at large temperatures it tends to zero. (d) Edge current vs. temperature, for $\mu = 0.2t_1$ and $3.2t_1$. When μ is small the edge current is stable against temperature. These results are obtained for a cylinder with $L_x \times L_y = 300 \times 30$.

between the vertices of a honeycomb lattice

$$H = \sum_{\langle ij \rangle} t_1 c_i^\dagger c_j + \sum_{\langle\langle ij \rangle\rangle} t_2 e^{i\nu_{ij}\phi} c_i^\dagger c_j + \sum_i V(\mathbf{r}_i) c_i^\dagger c_i. \quad (4)$$

A plaquette of this model is illustrated on Fig. 1a. It shows both undirected nearest neighbour hopping t_1 , as well as directed next-nearest neighbour hopping t_2 , with orientation indicated by the sign of $\nu_{ij} = \pm 1$, and a complex phase ϕ . Our model also includes a local potential $V(\mathbf{r})$ that can be constant or spatially varying. The Haldane model has two gapped topological phases with Chern numbers $\nu = +1$ and -1 , and trivial phase where $\nu = 0$. It is possible to cross between these phases by tuning ϕ, t_1, t_2 and V .

Without loss of generality, we show results for the topological insulator phase with $\nu = +1$, given by parameters $t_1 = 1$, $t_2 = 0.1$, $\phi = \pi/2$, for a cylinder with height L_y and circumference L_x . If the local potential depends only on the vertical coordinate $V(\mathbf{r}) = V(y)$, Hamiltonian (4) is a collection of L_x independent 1D problems, labeled by the momenta p_x around the cylinder. In the topological phase $\nu \neq 0$, the boundaries of the cylinder support gapless edge modes. There are two edge modes for each value of p_x , one for the top and one for the bottom boundary of the tube, as shown in Fig. 1(b). These gapless modes have an approximately linear dispersion relation $\omega \propto p_x$ and contribute to the total current that

runs parallel to the edge with opposite directions at the bottom and the top.

We can detect the edge currents in position space, by studying the flow of particles $n_i = c_i^\dagger c_i$. For a quadratic model $H = \sum_{ij} A_{ij} c_i^\dagger c_j$, the continuity equation reveals a set of currents J_{ij} running from site i to its neighbours

$$\frac{d}{dt} n_i = \sum_j J_{ij} \text{ with } J_{ij} = 2 \text{ Im} \left\{ A_{ij} \langle c_i^\dagger c_j \rangle \right\}. \quad (5)$$

Given a line “ l ” positioned perpendicularly to the boundary, such as the one in Fig. 1(b), we can compute the net particle flux due to the edge current from the ‘left’ (L) to the ‘right’ (R) as $I = \sum_{i \in L, j \in R} J_{ij}$. We observe that at low temperatures, $k_B T \ll t_1$, the net flux at the edge is a linear function of the chemical potential $V(\mathbf{r}) = \mu$ satisfying $I = \nu \mu / (2\pi)$, as shown in Figs. 1(c,d). We also observe that the current is invariant over a broad range of temperatures T , as expected for topological characteristics [21]. If the temperature or the chemical potential approaches the energy gap of the system, particles and holes in the conductance and valence bands wash out the topological protection and the current vanishes, as shown in Fig. 1(d).

Bulk currents in topological insulators:— We now explore the physics of a topological phase under the influence of inhomogeneous potentials, small enough that they do not cause any phase transition. Our first example is a cylinder with a step potential $V(\mathbf{r}) = w \text{ sign}(L_y/2 - y)$, taking different sign in the bottom and top half of the tube [cf. Fig. 2(a)]. In this setup we find three sets of localised currents, one at each of the two boundaries and one in the bulk. The edge currents run parallel to the boundaries of the tube. Due to (1) the edge currents are proportional to the local potential, which takes opposite sign on each boundary. So the edge currents now have the same orientation and grow as $I = |w|/(2\pi)$ [cf. Fig. 2(b)]. In addition to these currents, we find a surprising new bulk current localised at the potential jump, at $y = L_y/2$. This current flows opposite to the edge currents with twice their strength, $I = -2|w|/(2\pi)$, because it is proportional to the local potential gradient, $|\nabla V(\mathbf{r})| = 2|w|/a_0$, not to the local value of the potential itself.

Our study reveals that the bulk current is resilient to temperature changes, just like the edge currents [cf. Fig. 2(c)]. To further confirm their topological nature, we studied the resilience of all currents against local disorder. As anticipated, Fig. 2(d) shows that both edge and bulk currents are largely insensitive to local random potentials $V(\mathbf{r}) = w \text{ sign}(L_y/2 - y) + \epsilon$, with ϵ drawn with uniform probability from the interval $[-w_{\text{dis}}, w_{\text{dis}}]$. Note how the boundary of resilience is once more dictated by the energy gap of the topological insulator. Next, we want to verify the validity of Eq. (2), which gives the dependence of the bulk currents on the potential gradient.

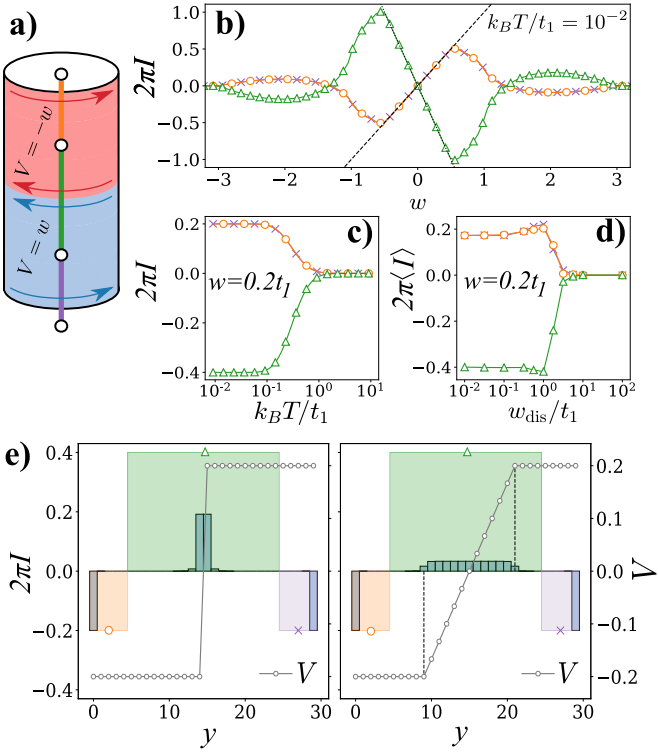


FIG. 2. Edge and bulk currents of the Haldane model with a step potential. As shown in (a), the bottom and top half of the cylinder have opposite potentials, $V(\mathbf{r}) = -w \text{sign}(L_y/2 - y)$. (b) Currents at both ends of the cylinder (crosses and circles) flow in the same direction and have equal magnitude $|w|/(2\pi)$. Bulk currents (triangles) localised at the $\pm w$ potential step flow in the opposite direction with twice the strength $2|w|/(2\pi)$. As with edge currents, bulk currents are robust against (c) temperature and (d) disorder (here $T = 0$). All data is presented for $\mu = 0$ on a cylinder with $L_x \times L_y = 300 \times 30$. Disorder is averaged over 100 samples and error bars on the mean $\langle I \rangle$ are too small to be visible. (e) Distribution of currents along the cylinder coordinate y (bars) for a step potential (left, line with dots) and for a linearly growing potential (right).

For that we determine the distribution of the current for a step potential and for a linearly varying potential along the cylinder. As expected, we find that the bulk current follows the potential gradient $\nabla V(\mathbf{r})$ in exact agreement with (2): it is localised at the position of the step for the step potential and it is constant along the ramp for the linear potential, as shown in Fig. 2(e).

Finally, note that both bulk and edge currents are localised. We can use the *inverse participation ratio* (IPR) to identify which eigenstates share this localisation and contribute to the currents [22]. For the n -th eigenstate ψ_{n,p_x} with quasimomentum p_x around the cylinder, the IPR is the higher moment of the wave function, $\text{IPR}_{n,p_x} = \sum_y |\psi_{n,p_x}(y)|^4$. Fig. 3 shows in colour how the localised states distribute across our energy bands. The edge states appear mostly in the band gap of the mate-

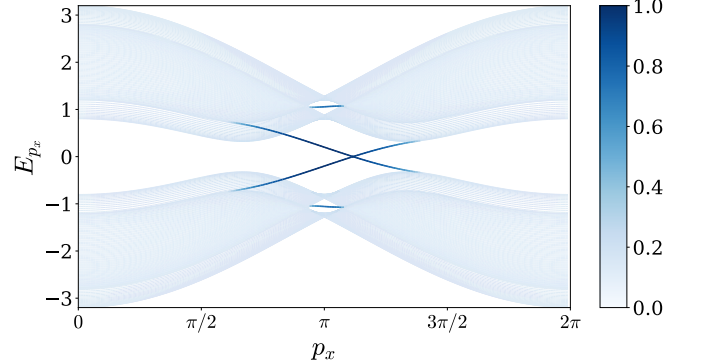


FIG. 3. Inverse participation ratios for the states on a cylinder. Eigenenergies of a cylinder with $L_x \times L_y = 120 \times 200$ sites are plotted as a function of the quasimomentum p_x , for a potential jump $w = 0.2t_1$. The colour of the line encodes the inverse participation ratio (IPR). In addition to the gapless edge states, localised states appear in the bulk due to the potential jump. These states support the bulk currents shown in Fig. 2.

rial. However, we also find highly localised states with energies well inside the bulk bands. These states give rise to the bulk currents right at the potential step.

Localised bulk states can be also generated in the 1D SSH topological model, which provides a more intuitive picture for their emergence. The SSH Hamiltonian with hopping t and potential V_i reads

$$H = -\frac{t}{2} \sum_i^{2L-1} [1 + \epsilon(-1)^i] c_{i+1}^\dagger c_i + \sum_i^{2L} V_i c_i^\dagger c_i. \quad (6)$$

In the perfectly dimerised regime $\epsilon = 1$ the system decouples into pairs of bound states $\frac{1}{\sqrt{2}}(c_{2i} + c_{2i+1})$ [cf. Fig. 4(a)], leaving two free edge states c_1 and c_{2L} . A potential step, $V_i = w \text{sign}(i - L)$ is invisible to most of the strongly coupled fermionic modes, except for the pair $\{c_L, c_{L+1}\}$ positioned at the step. As shown in Fig. 4(a), the potential step strains and progressively disentangles the pair $\{c_L, c_{L+1}\}$, causing the appearance of localised edge particle and hole states, the 1D equivalent of our bulk-currents. As in the cylinder, these new states sit in the bulk of the spectrum, with an energy $-\sqrt{w^2 + t^2}$ in between the bands $-t \pm w$ of the left and right half chains. To further demonstrate the disentangling caused by the potential step we consider the entanglement entropy of the left half of the chain as a function of w . We see that the entropy decreases monotonically with w away from its maximum values of $\ln(2)$ at $w = 0$, as shown in Fig. 4(b). Additionally, we see that the same generic behaviour also occurs away from pure dimerisation.

The SSH model is one of many topological phases that can be analysed using the theory of matrix-product-states [23–25]. These states or, more generally, tensor network states are written as the contraction of a network of tensors, one per site, with a connectivity that

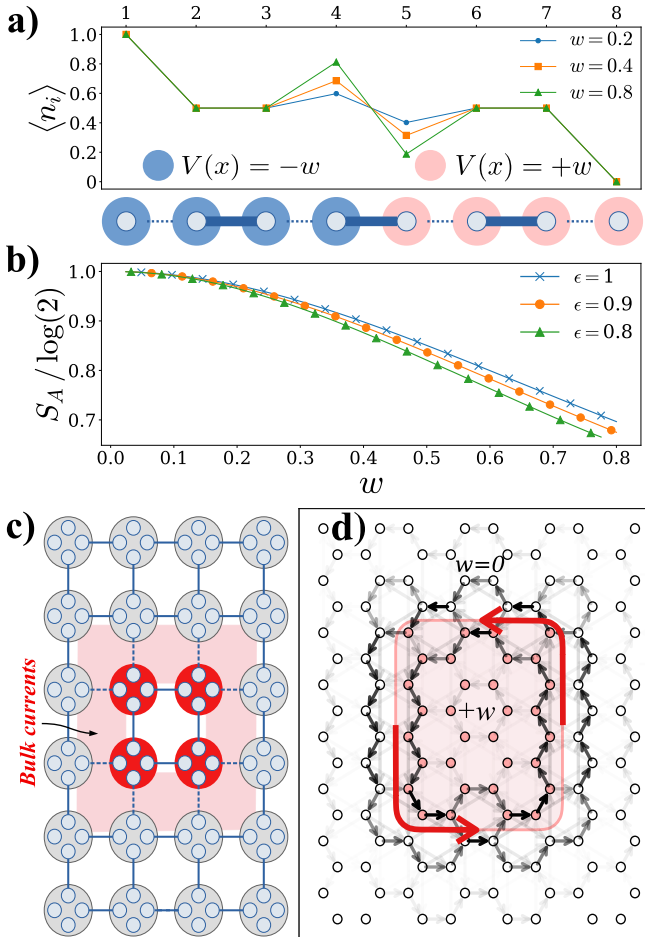


FIG. 4. Unbinding of bulk states. (a) We study the 1D SSH model with a local chemical potential $V(x) = w \text{ sign}(x - L/2)$, for a perfectly alternated hopping $J_{i,i+1} = t[1 + (-1)^i]$. Pairs of sites bind into dimers for $w = 0$. For increasing w the pair of modes at the potential step is progressively broken by the imbalance w , creating localised “bulk” particle and hole states. We show $w/t = 0.2, 0.4, 0.8$. (b) Entanglement entropy of region A (the half of the chain for which $V(x) = -w$) as a function of w . An increase in w progressively disentangles the two halves of the chain. Data presented for $t = 1$ and values of ϵ close to pure dimerisation. (c) A two-dimensional topological phase modelled after a tensor network representation. Hidden degrees of freedom bind to form a many-body entangled state. Unbound states on the boundary form an edge current. Similarly, the potential difference in the bulk partially disentangles those hidden “edge-like” states, creating a bulk current. (d) Homogeneous topological Haldane model, with a superimposed potential patch $V(x) = w = 0.1t_1$. Bulk currents appear around the patch, with magnitude and orientation controlled by w .

mimics the underlying lattice. In this representation, the contracted “legs” of the tensor act as hidden entangled states of the many-body system, which are correlated by the tensors, through a “projective measurement”. In the SSH model with $\epsilon = 1$ the representation is trivial and the “hidden” degrees of freedom map to the superposi-

tion states $c_{2i} + c_{2i-1}$ and the edge states $\{c_1, c_{2L}\}$ [cf. Fig. 4(a)].

If we abandon the fully dimerised limit $\epsilon \neq 1$ or move to two dimensions—e.g. the Haldane model—the fermionic topological phases require a more complex tensor network description [19]. As sketched in Fig. 4(c), general tensor network states have multiple entangled pairs correlated in an extended many-body state. The boundary of the topological model leaves unentangled degrees of freedom that can group into an edge state, with symmetry protected features. Also as in the SSH, any potential difference between neighbouring sites can strain the underlying entanglement, causing a partial decoupling of the tensors. This interpretation reveals a scenario where bulk currents can have tunable strength and direction, through a local control of the potential gradients across links in the lattice. As illustration, Fig. 4(d) shows the currents (arrows) on a 2D slab of the Haldane model, where we have $V(\mathbf{r}) = 0$ everywhere, except for a rectangular patch with $V(\mathbf{r}) = +w$. Note the emergence of localised currents around the border of the patch. The strength and orientation of the current can be controlled according to the law Eq. (2), and its direction adapts to the shape of the potential gradient.

Conclusions and outlook:— Summing up, we have found that the bulk of a topological insulator can exhibit robust, symmetry protected *bulk currents*. They share with edge currents an intrinsic robustness against temperature and local disorder. However, while edge currents are confined at the boundaries of the material, bulk currents are defined by gradients of local potentials and can adopt any shape, extension and strength. This means bulk currents can be used in the same applications as edge states, with greater versatility and without the need for complex sample fabrication and shaping. As a spin-off of this work, we have established a qualitative connection between the appearance of bulk currents and the theory of topological tensor network states. To our knowledge, the appearance of bulk currents is the first practical application of this theory and opens the door to further studies in more complex models, such as fermions with spin [1], topological superconductors or topological phases with interactions.

Acknowledgments:— We would like to thank Söfyan Iblisdir for the initial suggestion to investigate the edge currents of the Haldane model and for exciting conversations throughout the project. We would like to thank José Garré-Rubio for exciting conversations. This work was supported by the EPSRC grant EP/R020612/1, Spanish Projects PGC2018-094792-B-I00 (MCIU/AEI/FEDER, EU), PGC2018-094180-B-I00 (MCIU/AEI/FEDER, EU), FIS2015-63770-P (MINECO/FEDER, EU), CAM/FEDER Project No. S2018/TCS-4342 (QUITEMAD-CM) and CSIC Research Platform PTI-001. Statement of compliance with EPSRC policy framework on research data: This publica-

tion is theoretical work that does not require supporting research data.

[1] C. L. Kane and E. J. Mele, *Phys. Rev. Lett.* **95**, 226801 (2005).

[2] C. L. Kane and E. J. Mele, *Phys. Rev. Lett.* **95**, 146802 (2005).

[3] B. A. Bernevig and S.-C. Zhang, *Phys. Rev. Lett.* **96**, 106802 (2006).

[4] M. Z. Hasan and C. L. Kane, *Rev. Mod. Phys.* **82**, 3045 (2010).

[5] X.-L. Qi and S.-C. Zhang, *Rev. Mod. Phys.* **83**, 1057 (2011).

[6] H. Zhang, C.-X. Liu, X.-L. Qi, X. Dai, Z. Fang, and S.-C. Zhang, *Nature Physics* **5**, 438 EP (2009), article.

[7] D. Hsieh, D. Qian, L. Wray, Y. Xia, Y. S. Hor, R. J. Cava, and M. Z. Hasan, *Nature* **452**, 970 EP (2008).

[8] Y. L. Chen, J. G. Analytis, J.-H. Chu, Z. K. Liu, S.-K. Mo, X. L. Qi, H. J. Zhang, D. H. Lu, X. Dai, Z. Fang, S. C. Zhang, I. R. Fisher, Z. Hussain, and Z.-X. Shen, **325**, 178 (2009).

[9] M. Vergniory, L. Elcoro, C. Felser, N. Regnault, B. A. Bernevig, and Z. Wang, *Nature* **566**, 480 (2019).

[10] F. Tang, H. C. Po, A. Vishwanath, and X. Wan, **5** (2019), 10.1126/sciadv.aau8725.

[11] F. Tang, H. C. Po, A. Vishwanath, and X. Wan, *Nature* **566**, 486 (2019).

[12] S. Mondal, D. Sen, K. Sengupta, and R. Shankar, *Phys. Rev. Lett.* **104**, 046403 (2010).

[13] S. Zhang and X. Zhang, “Electrical and optical devices incorporating topological materials including topological insulators,” (2015), uS Patent 9,024,415.

[14] S. K. Banerjee, I. L. F. Register, A. MacDonald, B. R. Sahu, P. Jadaun, and J. Chang, “Topological insulator-based field-effect transistor,” (2014), uS Patent 8,629,427.

[15] B. Scharf, A. Matos-Abiague, J. E. Han, E. M. Hankiewicz, and I. Žutić, *Phys. Rev. Lett.* **117**, 166806 (2016).

[16] Y. Tanaka, T. Yokoyama, and N. Nagaosa, *Phys. Rev. Lett.* **103**, 107002 (2009).

[17] Y. D. Lensky, J. C. W. Song, P. Samutpraphoot, and L. S. Levitov, *Phys. Rev. Lett.* **114**, 256601 (2015).

[18] W. P. Su, J. R. Schrieffer, and A. J. Heeger, *Phys. Rev. Lett.* **42**, 1698 (1979).

[19] T. B. Wahl, H.-H. Tu, N. Schuch, and J. I. Cirac, *Phys. Rev. Lett.* **111**, 236805 (2013).

[20] F. D. M. Haldane, *Phys. Rev. Lett.* **61**, 2015 (1988).

[21] L. Leonforte, D. Valenti, B. Spagnolo, A. A. Dubkov, and A. Carollo, arXiv e-prints , arXiv:1905.04125 (2019), arXiv:1905.04125 [cond-mat.stat-mech].

[22] F. Evers and A. D. Mirlin, *Rev. Mod. Phys.* **80**, 1355 (2008).

[23] F. Pollmann, A. M. Turner, E. Berg, and M. Oshikawa, *Phys. Rev. B* **81**, 064439 (2010).

[24] X. Chen, Z.-C. Gu, and X.-G. Wen, *Phys. Rev. B* **83**, 035107 (2011).

[25] N. Schuch, D. Pérez-García, and I. Cirac, *Phys. Rev. B* **84**, 165139 (2011).